Journal of Power Sources 196 (2011) 3452–3460

Contents lists available at ScienceDirect

Journal of Power Sources

journal homepage: www.elsevier.com/locate/jpowsour

Hygro-thermal mechanical behavior of Nafion during constrained swelling

Meredith N. Silberstein, Mary C. Boyce*

MIT, Department of Mechanical Engineering, 77 Massaschusetts Avenue, Cambridge, MA 02139, United States

ARTICLE INFO

Article history:
Received 5 October 2010
Received in revised form
22 November 2010
Accepted 22 November 2010
Available online 7 December 2010

Keywords:
Polymer mechanics
Nafion
PEM fuel cells
PFSA membranes
Hygro-thermal coupling
Durability

ABSTRACT

Durability is a major limitation of current proton exchange membrane fuel cells. Mechanical stress due to hygro-thermal cycling is one failure mechanism of the polymer electrolyte membrane. In previous work the cyclic rate, temperature, and hydration dependent elastic–viscoplastic mechanical behavior of Nafion has been extensively investigated in uniaxial and biaxial tension, serving as a data basis and means of validation for a three-dimensional constitutive model. Here, the important effect of loading via constrained swelling is studied. Specifically, two types of loading are investigated: partially constrained swelling via a bimaterial swelling test and hygro-thermal cycling within a fuel cell. The bimaterial swelling conditions are examined via experiments in conjunction with modeling. Nafion/GDL bimaterial strips were hydrated and observed to curl significantly with the membrane on the convex side due to the large Nafion hygro-expansion coefficient. Upon drying the bimaterial strips developed a slight reverse curvature with the membrane on the concave side due to the plastic deformation which had occurred in the membrane during hydration. Finite element simulations utilizing the Nafion constitutive model successfully predicted the behavior during hydration and drying, providing insight on the constrained swelling physics and the ability of the model to predict such events. Simulations of in situ fuel cell hygro-thermal cycling are performed via a simplified two-dimensional fuel cell model. The simulation results confirm the finding of other studies that a tensile stress develops in the membrane during drying. Further, a concentration of negative hydrostatic pressure is found to develop just inside the channel region in the dried state supporting the theory of hygro-thermal driven mechanical stresses causing pinhole formation in the channel. The amplitude of the pressure cycling is found to be large and sensitive to both hygro-thermal ramp time and hold time. This finding is important for guiding both start-up and shut-down procedures and accelerated lifetime testing.

1. Background

The proton exchange membrane fuel cell (PEMFC) is a promising clean technology for converting chemical energy into electrical energy, particularly for transportation. Insufficient durability is one of the major factors inhibiting the widespread distribution of this technology. In particular, the membrane electrode assembly (MEA), which consists of a selectively permeable polymer electrolyte membrane (PEM) with a catalyst layer and porous carbon electrode support on each side, is known to fail under the cyclic operating conditions of automobiles. The PEM is responsible for conducting protons while preventing hydrogen and oxygen gas crossover. Until recently, durability research has focused on preventing degradation due to chemical attacks, however, with progress against chemical attacks focus has shifted to the increasingly significant mechanical degradation modes [1]. Cyclic mechanical loading results from water content driven swelling and deswelling of the membrane within the partially constrained environment of the fuel cell. Gas crossover has been seen to develop across membranes in fuel cells subjected only to relative humidity cycling. In particular, it was found that pinholes develop in the membrane regime bordering the channel of the bipolar plates [2]. The current PEM benchmark Nafion, a perfluorosulfonated ionomer manufactured by Du Pont, is taken as a representative membrane for understanding this failure mechanism.

In our prior work [3] the uniaxial tensile behavior of Nafion was characterized under both monotonic and cyclic loading as a function of rate, temperature, and hydration. Based on this data a constitutive model was created to describe the hygro-thermal elastic–viscoplastic stress–strain behavior of Nafion. The model was shown to capture the stress–strain behavior of Nafion over a wide range of uniaxial loadings histories [3] and later shown to accurately predict the stress–strain behavior of Nafion over a range of biaxial loading histories [4]. This paper explores the constrained swelling induced and hydration dependent mechanical response of

* Corresponding author at: Massachusetts Institute of Technology, Mechanical Engineering, Room 1-025, 77 Massachusetts Ave, Cambridge, MA 02139, United States. Tel.: +1 617 253 5087; fax: +1 617 258 8742.
E-mail addresses: meri.silberstein@gmail.com (M.N. Silberstein), mcboyce@mit.edu (M.C. Boyce).

0378-7753/$ – see front matter © 2010 Elsevier B.V. All rights reserved.
doi:10.1016/j.jpowsour.2010.11.116

the material and the model. Bimaterial swelling tests are conducted on the membrane bonded to a gas diffusion layer material, which provides a constrained state of the membrane upon hydration and produces membrane stresses and a measurable deformation, the curvature of the bilayer. The ability of the model to predict constrained swelling loading conditions is assessed with respect to these experiments. The validated model is then applied to a simplified fuel cell duty cycle in order to understand and predict stress and strain evolution and potential failure mechanisms of membranes in operating fuel cells.

2. Experimental methods

2.1. Materials

Commercially available dispersion cast NRE211 films (thickness $t = 27\,\mu m$, Dupont, Ion Power Inc.) and NRE212 films (thickness $t = 54\,\mu m$, Dupont, Ion Power Inc.) were used for the experimental characterization of Nafion. The films were stored in a desiccator cabinet upon removal from the initial packaging to minimize variability in data from aging and humidity effects.

Commercially available LT 1200-N (thickness $t = 180\,\mu m$, E-Tek, Fuel Cell Store) was used for the GDL material for the bimaterial swelling tests.

2.2. Uniaxial tension

Uniaxial tension tests were conducted on Nafion NRE212 under monotonic, cyclic, stress relaxation, and creep histories, at constant engineering strain rates from $00.1\,s^{-1}$ to $0.1\,s^{-1}$, at temperatures from 25 °C to 100 °C, and at various water contents [3].

2.3. Biaxial tension

Biaxial tests were performed on Nafion NRE211 laser cut into a cruciform shape. Biaxial tests were conducted on the thin film multi-axial tensile machine developed in the Bio-Instrumentation lab at MIT modified from the design of Herrmann [4,5].

2.4. Bimaterial swelling

Bimaterial specimens were prepared by hot pressing Nafion (NRE211 and NRE212) onto a single piece of GDL (thickness $t = 180\,\mu m$, E-Tek LT 1200-N) at 120 °C for 5 min. Specimens were then cut to 1.5 mm × 15 mm strips with a razor guided by a straight edge. One end of the specimen was clamped into Zwick screw grips such that 5 mm of the specimen remained unclamped (Fig. 1). The specimen was then sprayed with deionized water from the GDL side. The deformation was imaged over 5 h via a Qimaging Retiga 1300 camera.

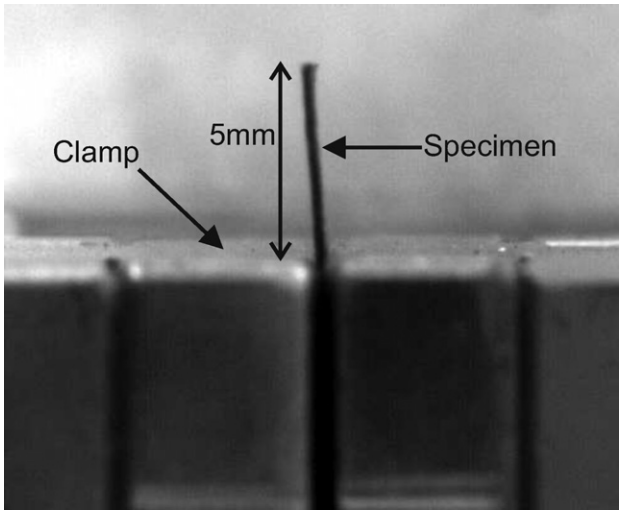

Fig. 1. Experimental setup for bimaterial test.

3. Constitutive model review

In prior work of the authors, a three-dimensional constitutive model for Nafion was developed and implemented as a user material subroutine in the finite element program Abaqus [3]. Monotonic and cyclic uniaxial tension experiments over a range in strain rates and environmental conditions were used to fit and validate the model. This model and the experimentally observed uniaxial behavior will be briefly reviewed here to facilitate understanding of the results.

The elastic–viscoplastic constitutive model is depicted rheologically in Fig. 2, it consists of an intermolecular deformation mechanism (Mechanism I) acting in parallel with a molecular network alignment mechanism (Mechanism N). The intermolecular mechanism, rheologically depicted as an elastic spring in series with a viscoplastic dashpot (P), represents the resistance to deformation due to the intermolecular interactions where the spring captures the stiffness of these interactions and the nonlinear dashpot captures the yielding of these interactions. The intermolecular mechanism has a back stress (B) on the viscoplastic element which develops during loading to assist inelastic recovery. The network mechanism is a nonlinear spring which captures the resistance due to the stretching and orientation of the molecular network. The intermolecular resistance is strongly dependent on temperature and hydration, decreasing significantly when the polymer goes from the glassy state into the glass–rubber transition regime (~60–120 °C). The network resistance is operational at all temperatures. The hygro-thermal swelling, which is assumed to be both linear and isotropic, is a source of inelastic deformation within the intermolecular leg.

A summary of results from this model compared with uniaxial tensile experimental data is shown in Fig. 3. The model is able to capture the linear-elastic response, the rate dependent distributed yield event, and the nonlinear strain hardening under monotonic and cyclic tensile loading. Additionally it is able to capture the nonlinear unloading and reloading observed to be characteristic of cyclic loading both as a function of strain and as a function of strain rate. The linear superposition of the effects of temperature and water content (captured as moles of water per mole of sulfonic acid group as typical in the Nafion literature, here called ϕ) is seen to work well. The cyclic behavior remains qualitatively the same with

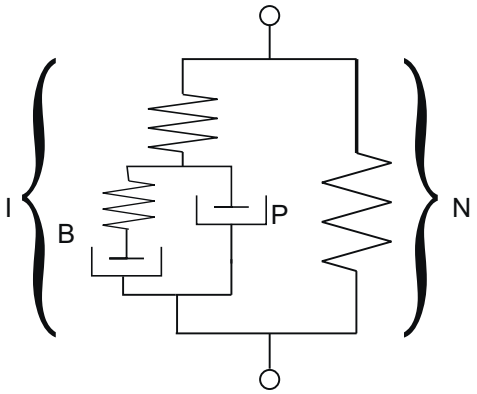

Fig. 2. Rheological depiction of Nafion constitutive model.

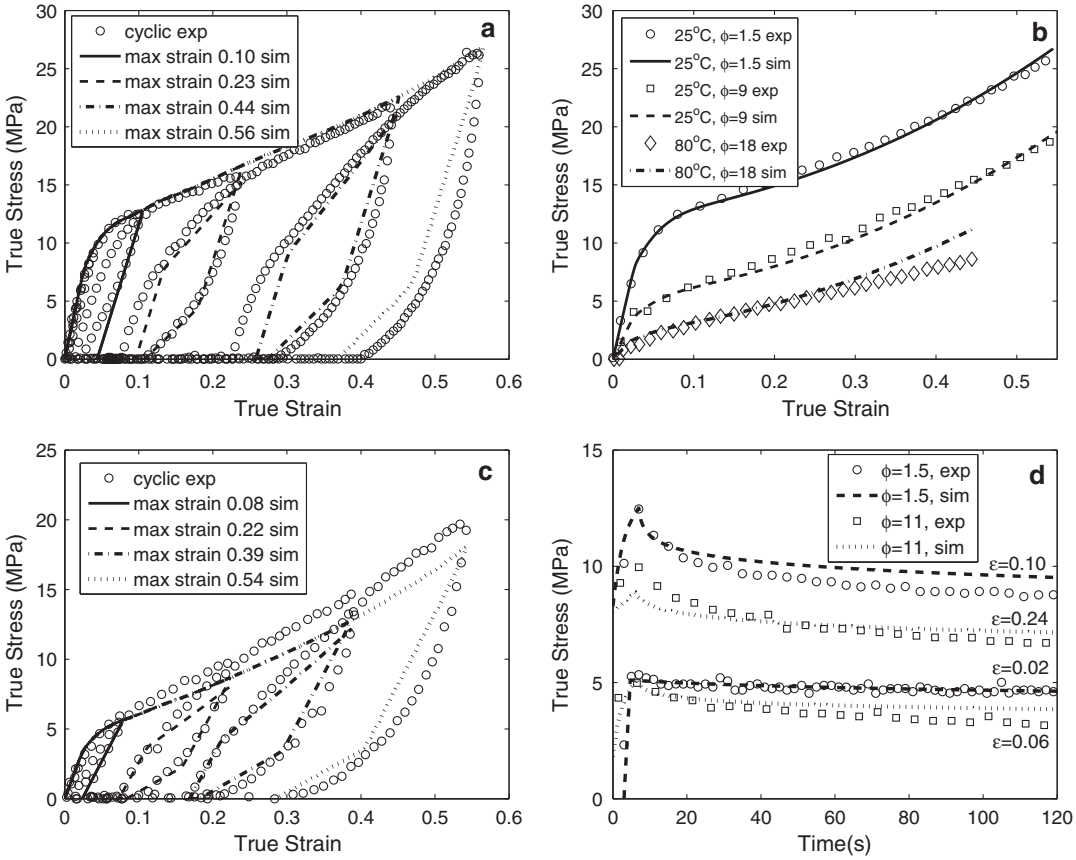

Fig. 3. Comparison of constitutive model predictions with experimental data for uniaxial tensile loading of NRE212: (a) cyclic behavior at different maximum strains at ambient conditions (25 °C, $\phi = 1.5$), (b) monotonic behavior as a function of temperature and hydration, (c) cyclic behavior at different maximum strains in water (25 °C, $\phi = 11$), (d) stress relaxation in air and water (25 °C).
(a–c) Reprinted from Silberstein and Boyce 2010 [3].

changes in temperature and hydration and is well captured by the same stiffness and yield dependence that governs the monotonic behavior. The evolution of stress relaxation and creep (not shown) through yield are also well predicted by the model.

A summary of results from the model compared with experimental data from biaxial tensile tests conducted on cruciform specimens is shown in Fig. 4. The degree of biaxiality B is defined as the rate of applied extension in the 1-direction over the rate of applied extension in the 2-direction. The specimen exhibits an elastic–plastic response with features similar to the uniaxial behavior. The biaxial effect on the stress–strain response is apparent. In the 2-direction both the stiffness and the yield stress increase with increasing degree of biaxiality. The stress response in the 1-direction decreases as expected with decreasing degree of biaxiality since there is less strain applied in that direction. The simulations well capture the initial stiffness, the yield, and the post-yield behavior as observed for 1- and 2-direction stress–strain histories for differing degrees of biaxiality, indicating high accuracy of the model for biaxial loading. The cyclic behavior (not shown) is qualitatively similar to the uniaxial cyclic behavior: there is a non-linear unloading and reloading with a reduced yield upon reloading. The cyclic behavior is also captured by the model [4]. We can see that the framework used to incorporate the uniaxial behavior into a three-dimensional model is in fact capable of predicting the multiaxial deformation response of the membrane.

4. Bimaterial testing results and discussion

The swelling of a bimaterial Nafion/GDL strip was chosen to interrogate the constrained swelling-induced and hydration dependent mechanical stress aspects of Nafion behavior and to assess the ability of the constitutive model to capture this behavior. When water is sprayed on the bilayer, the Nafion membrane will attempt to swell in all directions, but the GDL will constrain expansion in the membrane plane, creating a net compressive force in the membrane and a net tensile force on the GDL which must balance to satisfy force and moment equilibrium. These compatibility and equilibrium conditions will cause the composite bilayer strip to curl, much as the thermostat bimetallic strips with mismatched thermal expansion coefficients bend upon a change in temperature. The bimaterial test has recently been used to estimate the level of stress experienced by the membrane due to constrained swelling [6]. This method required the choice of a substrate with targeted elastic properties to enable an analytical reduction of the data. Here, the constrained swelling of Nafion bonded to a typical GDL substrate is examined.

Representative images of the NRE212/GDL strip with membrane thickness 54 μm are shown before testing, while hydrated, and after drying in Fig. 5. The hydrated state is achieved on the order of seconds, while the drying occurs over 5 h with most of the drying occurring during the first half hour. This drying rate is influenced by water that collects within the clamp. Upon hydration, the bimaterial strip is observed to curl with the GDL on the concave side and then to gradually straighten during drying, eventually curling in the reverse direction with the membrane on the concave side. This reverse direction curling can be attributed to the plastic deformation that occurs within the membrane during the constrained swelling process. If the swelling deformation were fully elastic the bimaterial strip would have no curvature in the final state. The radii of curvatures in the hydrated and dried state

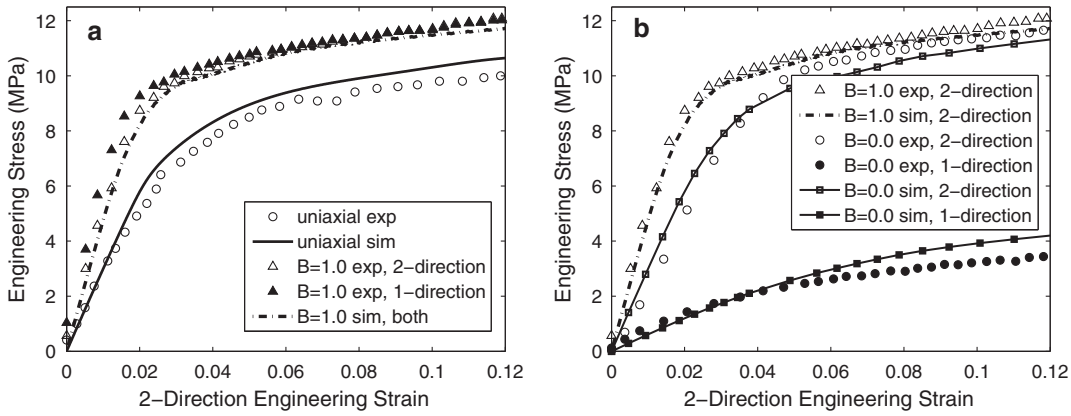

Fig. 4. Model compared to experimental data for biaxial tensile loading of NRE211 using video extensometer equivalent strain measure: (a) comparison of uniaxial ($B \sim -0.5$) and equibiaxial ($B = 1.0$), (b) comparison of equibiaxial ($B = 1.0$) and "fixed" biaxial ($B = 0.0$).

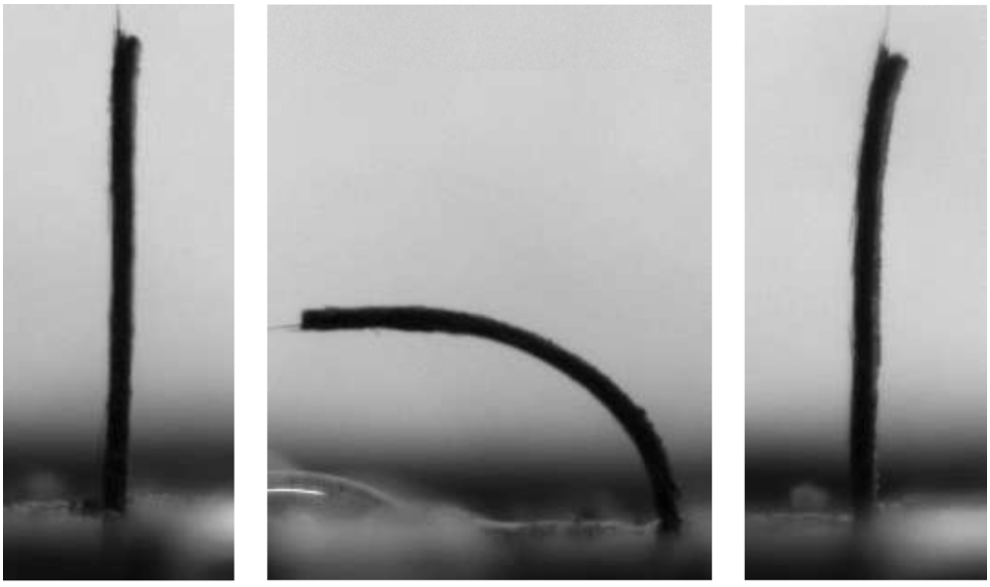

Fig. 5. Images of NRE212 bimaterial swelling test ($t_{NRE212} = 54\ \mu m$, $t_{GDL} = 180\ \mu m$): (a) Initial configuration, (b) hydrated and (c) dried. Nafion is on the right side of the strip.

are given in Table 1 along with the corresponding standard deviation.

Table 1 also shows the results for the case of the Nafion NRE211/GDL bilayer where membrane thickness is 27 μm; representative images are given in Fig. 6. It can be seen that the reduction in membrane thickness results in a decrease in curvature in the hydrated state by a factor of two, scaling roughly with membrane thickness.

The Stoney formula [7] provides an expression for the curvature (k) of a bilayer of a substrate with a stressed thin film:

$$\kappa = \frac{6f}{E_s h_s^2} \tag{1}$$

where f is the film force per unit membrane width, E_s is the substrate modulus, and h_s is the substrate thickness. The film force is a result of a strain mismatch with the substrate (in this case, a result of swelling mismatch). The stress may arise from elastic or inelastic behavior of the membrane where the force is the product of the average membrane stress and the membrane thickness. For the case where the membrane is elastic-perfectly plastic with yield stress $\sigma_{y,f}$, $f = \sigma_{y,f} h_f$. Eq. (1) then provides a simple relationship to either obtain the curvature given the material behavior or to obtain the membrane force given the curvature. Considering the membrane to have yielded, Eq. (1) then indicates a factor of two difference in curvature for the two thicknesses considered here which is in good agreement with our measurements. The factor of two arising simply

Table 1
Experimental and simulation results of bimaterial swelling test.

Material	State	Experiment Radius (mm)	Curvature (m^{-1})	Standard deviation (%)	Simulation Curvature (m^{-1})	Error (%)
NRE212	Hydrated ($\phi = 9.5$)	6.8	148	7.4	134	9.5
($t = 54\ \mu m$)	Dried ($\phi = 1.5$)	29	35	34	34	2.9
NRE211	Hydrated ($\phi = 9.5$)	14	72	28	73	1.4
($t = 27\ \mu m$)	Dried ($\phi = 1.5$)	33	30	19	28	6.7

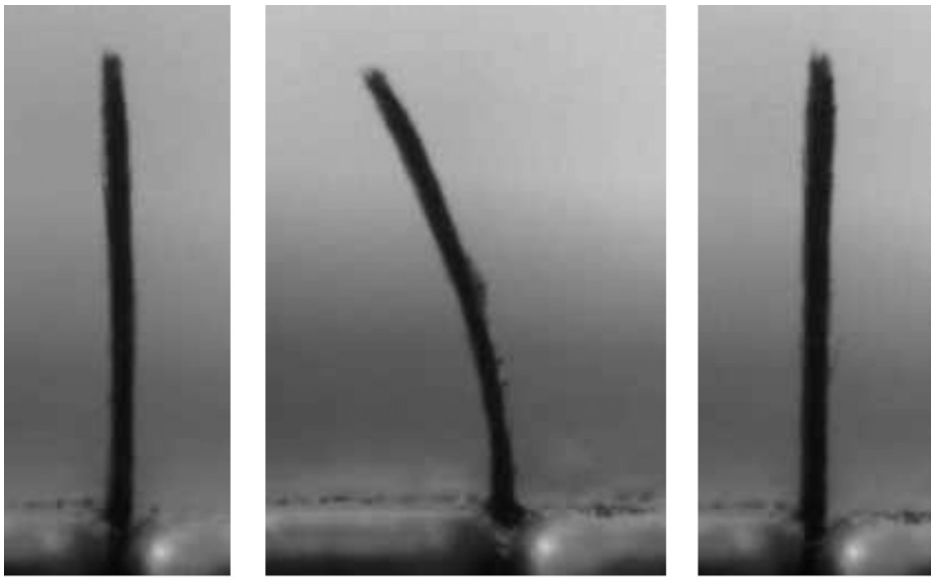

Fig. 6. Images of NRE211 bimaterial swelling test (t_{NRE211} = 27 μm, t_{GDL} = 180 μm): (a) initial configuration, (b) hydrated and (c) dried. Nafion is on the right side of the strip.

due to the membrane force scaling directly with thickness. Quantitatively, considering the membrane to have yielded at a hydrated yield stress of 5 MPa, Eq. (1) predicts $k = 139\ \mathrm{m}^{-1}$ for $h_f = 27\ \mu\mathrm{m}$ and $k = 278\ \mathrm{m}^{-1}$ for $h_f = 54\ \mu\mathrm{m}$ which overpredict the observed curvatures.

Taking into account the fact that the film is not thin relative to the substrate, for the case where the film has fully yielded and the membrane is approximated as elastic-perfectly plastic, the curvature is given by:

$$\kappa = \frac{6\sigma_{y,f}}{h_s E_s} m\eta(1+\eta) \tag{2}$$

where $m = E_f/E_s$ is the elastic modulus ratio and $\eta = h_f/h_s$ is the thickness ratio. Eq. (2) predicts $k = 62\ \mathrm{m}^{-1}$ for $h_f = 27\ \mu\mathrm{m}$ and $k = 140\ \mathrm{m}^{-1}$ for $h_f = 54\ \mu\mathrm{m}$ which is quite similar to the experimental result. This analysis neglects secondary effects of the biaxiality of the loading that results from the finite depth of the specimen (1.5 mm) which would decrease the curvature and of strain hardening of the membrane which would increase the curvature.

The dried curvature is sensitive to the length of time the strip is hydrated since it is a function of the rate dependent plasticity. It will be discussed in more depth with respect to the finite element simulations.

The constitutive model together with the nonlinear finite element method is used to simulate the bilayer swelling. The GDL is assumed to be linear elastic, characterized by an elastic modulus of 180 MPa and a Poisson's ratio of 0.25; furthermore, the GDL does not swell. The membrane is modeled to hydrate over a time period of 10 s, held hydrated for 300 s, and then dried exponentially over 3600 s (with time constant $\tau = 500$ s) for NRE212 and 1800 s (with time constant $\tau = 250$ s) for NRE211. Exponential drying is chosen based on the work of Satterfield and Benziger [8] which shows that water desorption is controlled by interfacial mass transport. The drying is taken to occur twice as fast for NRE211 since desorption time is directly proportional to thickness.

Side view images from the 3D finite element simulation results are shown before testing, while hydrated, and after drying, for NRE212 (Fig. 7) and for NRE211(Fig. 8). It is evident that the simulation matches the experiment qualitatively with the hydrated curvature for NRE212 approximately twice that for NRE211 and the dried curvature similar for each. In the hydrated state the stress is compressive throughout the membrane and the magnitude indicates the membrane has yielded (Fig. 9a). The nonlinearity in the membrane stress distribution results from plastic deformation. Stress in the GDL is compressive at the outer surface and increases linearly, becoming tensile as it approaches the interface with the membrane. The axis of zero strain is seen to be quite close to the outer surface. In the dried state, the residual stress in the membrane is tensile and mirrors the shape of the hydrated stress but is smaller in magnitude. The stress in the GDL is mostly compressive but is slightly tensile at the outer surface and is significantly lower than in the hydrated state. Table 1 shows that the hydrated and dried curvatures predicted by the model for both NRE212 and NRE211 show excellent quantitative agreement with the experimental data. This indicates that the constitutive model successfully captures and predicts the swelling kinematics and the effect of swelling on the elastic–plastic behavior.

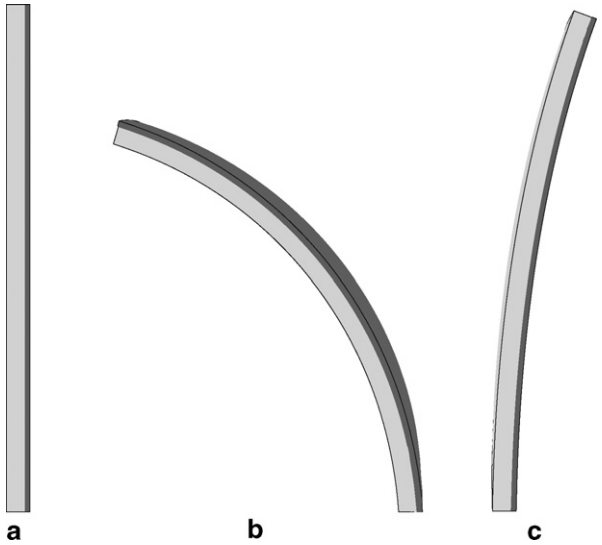

Fig. 7. Side view images of the finite element simulation of bimaterial swelling test with NRE212: (a) initial configuration, (b) hydrated and (c) dried. Nafion is indicated by dark grey, the GDL is indicated by light grey.

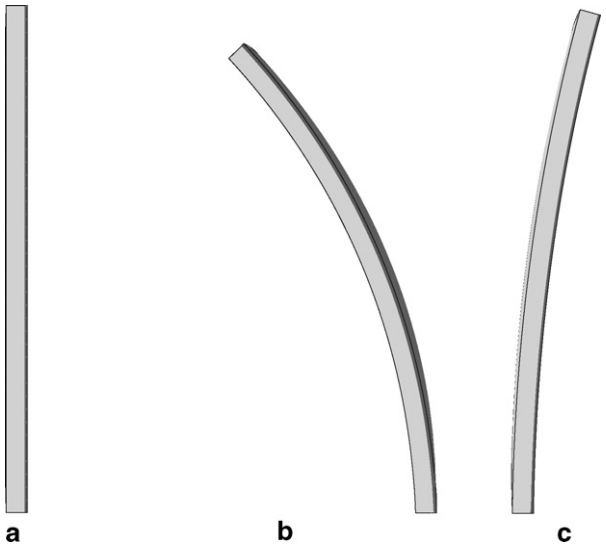

Fig. 8. Side view images of the finite element simulation of bimaterial swelling test with NRE211: (a) initial configuration, (b) hydrated and (c) dried. Nafion is indicated by dark grey, the GDL is indicated by light grey.

5. In situ fuel cell application of model

The constitutive model has been shown to be effective in predicting cyclic and rate dependent uniaxial stress–strain behavior, biaxial stress–strain behavior, and bilayer curvature induced by constrained swelling. The model is now applied with confidence to simulate the behavior of Nafion within the constrained loading conditions of a fuel cell. Several groups have simulated in situ membrane loading using alternative Nafion constitutive models. Karlsson and coworkers used first a linear-elastic and then elastic–plastic models with thermal and hygro-expansion to simulate a membrane within a two-dimensional (assuming plane strain in the third direction) fuel cell unit consisting of a land and a channel region of the bipolar plate sandwiching an MEA. They explored fixed displacement and fixed load boundary conditions on the bipolar plates for both aligned and un-aligned channels. Their results showed two key findings when the unit was subjected to hygro-thermal cycling: (i) normal stresses are significantly larger than shear stresses; (ii) when plasticity is included in the material model, tensile stresses develop upon dehydration [9–11]. Solasi et al. simulated the fuel cell as an elastic–plastic membrane subjected to fixed boundary constraints on all four sides and free to expand in the through-plane direction. They found that the stress evolution is a complicated combination of the swelling due to hydration and the change in properties due to temperature and hydration changes [12]. Lai et al.[2] performed a similar simulation using a viscoelastic membrane constitutive model. They found that the stress was tensile during drying, that the peak tensile stress increased with each cycle, that its value depended on the rate of hydration/dehydration, and that its value exceeded that of the yield stress suggesting the need for a viscoplastic model. The work presented here employs a geometry similar to that of Karlsson and coworkers in order to study the stress and strain non-uniformity across the channel and land; following the findings of these previous studies attention will be drawn to normal stresses in the dried state and the effect of multiple cycles.

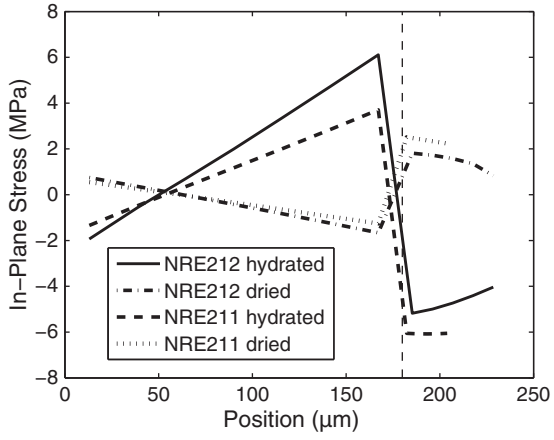

Fig. 9. Stress profile across bimaterial strip (thin dashed line indicates GDL/Nafion border).

The geometry used in these simulations is shown in Fig 10a; the 25 μm thick membrane is perfectly bonded to 100 μm thick gas diffusion layers to form the sandwiched membrane electrode assembly (MEA). The MEA is placed within aligned bipolar plates, the land and the vertically open channel are each 0.5 mm. The repeating nature of the unit cell is captured with symmetry boundary conditions where the MEA is not allowed to expand or contract in the horizontal direction. The bipolar plates are subject to a constant force in the vertical direction of 1 N per unit mm depth corresponding to a nominal stress of 1 MPa per total area or 2 MPa per contact area. (The results were found to be qualitatively insensitive to the force applied to the bipolar plates.) Plane strain is assumed in the third dimension, creating a biaxial loading condition in the membrane plane. The bipolar plates are taken to be rigid and the gas diffusion layers are modeled as isotropic linear elastic defined by elastic modulus 180 MPa and Poisson's ratio 0.25. While available data suggests that the typical GDL mechanical behavior is neither isotropic nor linear [13,14], parametric studies showed these results to be relatively insensitive to a reasonable modulus range and to anisotropy in the GDL given the constant vertical force constraint and the horizontal membrane constraint imposed by the rigid bipolar plates. The membrane is subjected to a uniform history of water content and temperature changes as shown in Fig. 10b where the water content is varied from 1.5 to 22 and the temperature is varied from 25 °C to 85 °C. Recent simulations by Kusoglu et al. suggest that a uniform hydration assumption would be reasonable under open circuit voltage conditions where electro-osmotic drag does not factor in [11].

When the membrane is hydrated within the fuel cell, the constraints of the GDL and the bipolar plate inhibit the swelling, resulting in significant stress (σ) in the membrane. Representative σ_{11} and σ_{22} contours for the hydrated state are shown in Fig. 11a top and bottom, respectively. The membrane experiences compressive stress in both the 1- and 2-directions. σ_{22} is largest beneath the land where the membrane is directly compressed by the clamping force essentially giving a compressive stress of 2 MPa. Typical σ_{11} and σ_{22} contours for the dried state are shown in Fig. 11b top and bottom, respectively. σ_{22} is compressive and again largely dependent on the applied force constraint. σ_{11} is tensile throughout the membrane and largest just inside the channel. This tensile stress arises due to prior plastic deformation of the membrane during the hydration process. The plastic strain (ε^p) in the hydrated and dried states is shown in Fig. 12. In both states ε^p_{11} is negative throughout the membrane and ε^p_{22} is positive throughout the membrane. Both of these components of the plastic strain are greater in the channel as a result of the reduced constraint/pressure and larger Mises stress, this effect is more exaggerated for a larger constant force constraint (not shown). The development of plastic strain and the resulting tensile stress during cycling strongly supports the concept of mechanically driven membrane failure in fuel cells. One of the more subtle aspects of this in situ modeling is that while

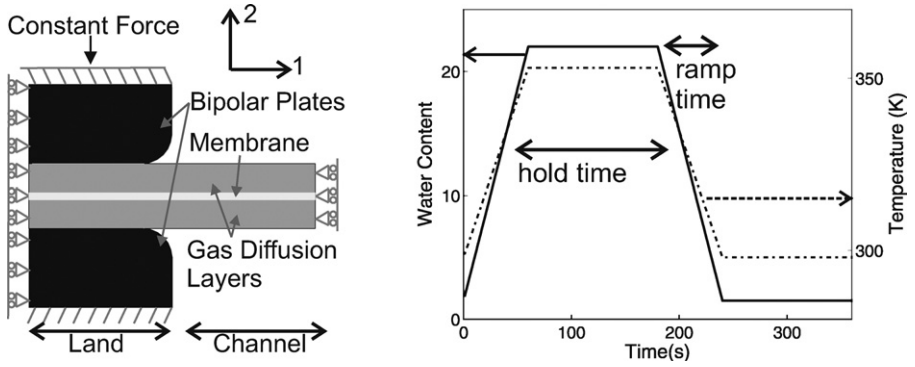

Fig. 10. In situ fuel cell simulation: (a) geometry and boundary constraints and (b) applied water content and temperature loading.

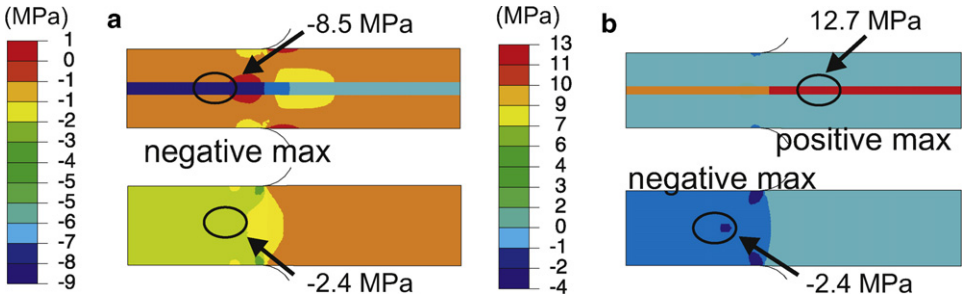

Fig. 11. Typical stress contours during hygro-thermal cyclic loading: (a) hydrated, (b) dried. Top: σ_{11}, bottom: σ_{22}.

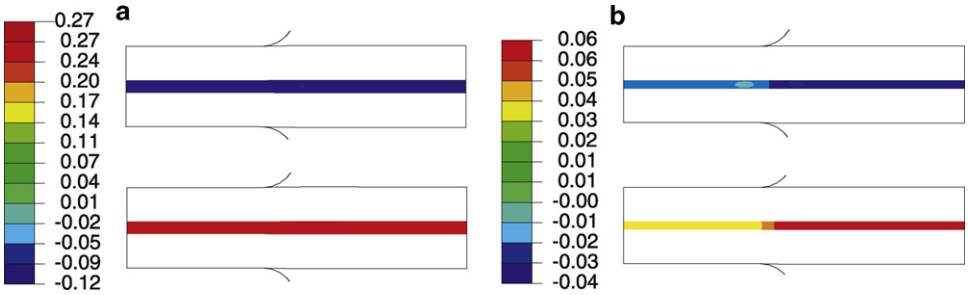

Fig. 12. Typical plastic strain contours during hygro-thermal cyclic loading: (a) hydrated and (b) dried. Top: ε^p_{11}, bottom: ε^p_{22}.

the hydration process causes swelling strains, the elastic and plastic properties of the membrane are being reduced as a result of the increase of the water content and temperature. Consequently, similar magnitude stress levels in the hydrated and dried states are likely to cause more plastic deformation in the hydrated state.

For completeness σ_{33} and σ_{12} contours are also included for the hydrated and dried states (Fig. 13). σ_{33}, which results from the plane strain boundary condition in the 3-direction, is quite similar to σ_{11}. σ_{33} is compressive throughout the membrane in the hydrated state and tensile throughout in the dried state. In both states the stress is more positive (tensile) in the channel than in the land. This reaffirms: (1) that the 1-direction constraint imposed by the rigidity of the bipolar plates is equivalent to plane strain with stress and strain variation arising from the 2-direction boundary variation; and (2) that the in situ loading is biaxial. Although failure is not explicitly modeled here it is useful to compare this biaxial stress, which is on the order of 10 MPa in the dried state, with that shown to cause failure in the literature. Pressure blister tests

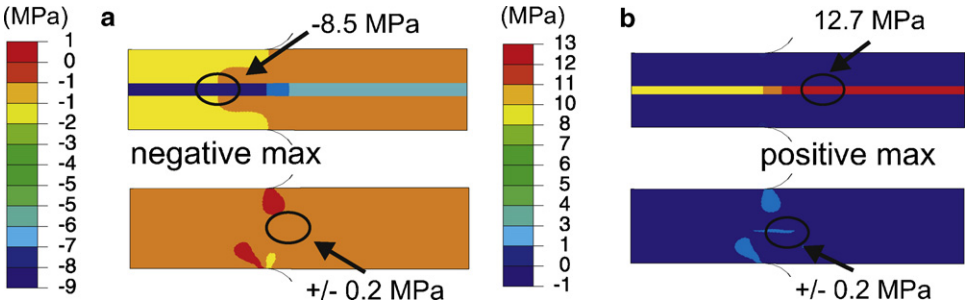

Fig. 13. Typical stress contours during hygro-thermal cyclic loading: (a) hydrated and (b) dried. Top: σ_{33}, bottom: σ_{12}.

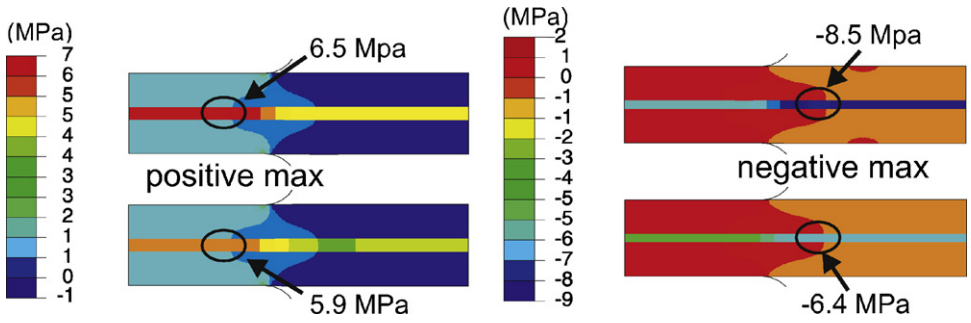

Fig. 14. Typical hydrostatic pressure contours during hygro-thermal cyclic loading: (a) hydrated and (b) dried. top: when environmental state first reached, bottom: after held at environmental state for 60 s.

conducted on NRE211 at 80 °C and 2%*RH* show that leaks occur at around 100 s when the biaxial stress is held at 10 MPa and around 10,000 s when the biaxial stress is held at 2 MPa [15]. While these environmental conditions do not match those used in the fuel cell simulation, and the 2-direction stress may significantly contribute to inhibiting failure, it is clear that the biaxial stresses reached during in situ hygro-thermal cycling are large in comparison to the fatigue failure criteria. The shear stress σ_{12} is at a maximum right around the land/channel interface however, it is negligible in comparison to the normal stresses in both the hydrated and dried states. σ_{12} never exceeds 0.2 MPa compared to 2 MPa typical for σ_{22} and 10 MPa typical for σ_{11} and σ_{33}.

In the literature, membrane failure is primarily discussed in terms of either pinhole formation or membrane thinning (i.e. [1]). These arise from a combination of mechanical and chemical damage and are presumably coupled in their development, but nominally, one could affiliate pinhole formation with some form of cavitation or crazing event resulting from negative hydrostatic pressure [16]. Focus will now be directed to the negative hydrostatic pressure as an indicator of potential membrane failure. The pressure evolution will be followed through a single hydration/drying cycle and then through multiple cycles as a function of hydrating and drying rates and hold times at each state. The pressure develops similarly to the σ_{11} stress; in the hydrated state the pressure is positive (compressive) and in the dried state the pressure is negative (tensile). Typical contours for these two states are shown in Fig. 14a and b top. In the hydrated state the pressure is greatest under the land. In the dried state there is a negative pressure concentration that develops just inside the channel; this is where cavitation or crazing would be expected to occur. Fig. 15 shows the pressure history in the membrane in the channel region just outside the land where the maximum negative value occurs and also shows the history of σ_{11} in this same area, revealing the cycling between compressive and tensile states. The pressure in this region cycles from ~4 MPa in the hydrated state to ~–8 MPa in the dried state. In both the hydrated and dried states the pressure relaxes with time and becomes more uniform as the membrane is held at constant environmental conditions (Fig. 14a and,b bottom). The time scale of this relaxation is linked to the intrinsic relaxation of the material as characterized in uniaxial experiments. Most of the relaxation occurs over the first 30 s with the pressure approaching a steady state. Since the pressure has its greatest negative value immediately after drying/cooling is finished, the pressure at this point in the first and tenth cycles will be used to track the effect of ramp rate and hold time on pressure of the in situ membrane (Fig. 16). Increasing the ramp time (decreasing the ramp rate) decreases the peak pressure for both the first and tenth cycles as this increases the time the membrane has to relax in response to the applied hygro-thermal load. Increasing the hold time increases the peak pressure for the first cycle but decreases the peak pressure for the tenth cycle. This counterintuitive result can be explained by the fact that relaxation that occurs in the hydrated state will drive the magnitude of the negative pressure to increase while relaxation that occurs in the dried state will drive the magnitude of the negative pressure to decrease, at the first cycle negative peak only the former will have occurred. Across the board the tenth cycle pressure is below that of the initial cycle.

In accelerated mechanical lifetime testing, a particular relative humidity and temperature cycle is applied to the membrane within the fuel cell. It is assumed that these short cycles are equivalent to operating cycles, but it is unclear whether this is an effective method of assessing mechanical durability of a membrane [15]. These in situ simulations show that in order to properly reproduce the peak pressure, the ramp up and ramp down times in the accelerated test must match the startup and shutdown times in an operational fuel cell. The choice of hold time is less clear since

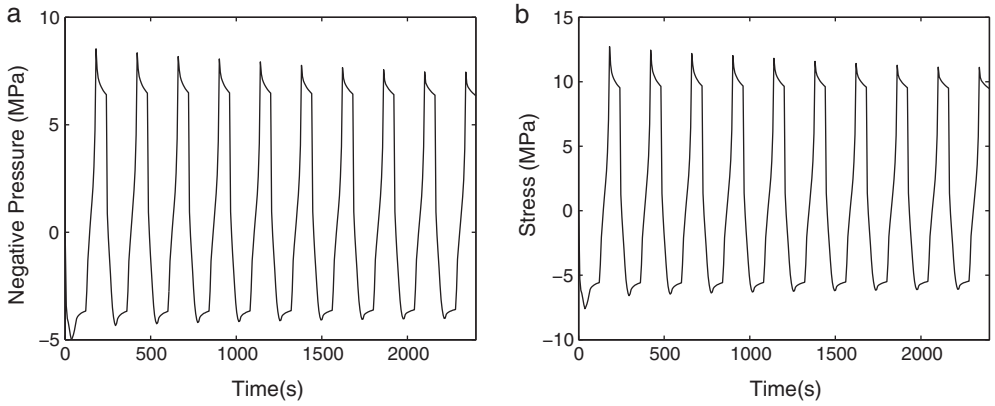

Fig. 15. Evolution of stress values at the concentrated location just inside the channel during hygro-thermal cyclic loading when ramped over 60 s and held at each state for 60 s (a) negative hydrostatic pressure (b) σ_{11}.

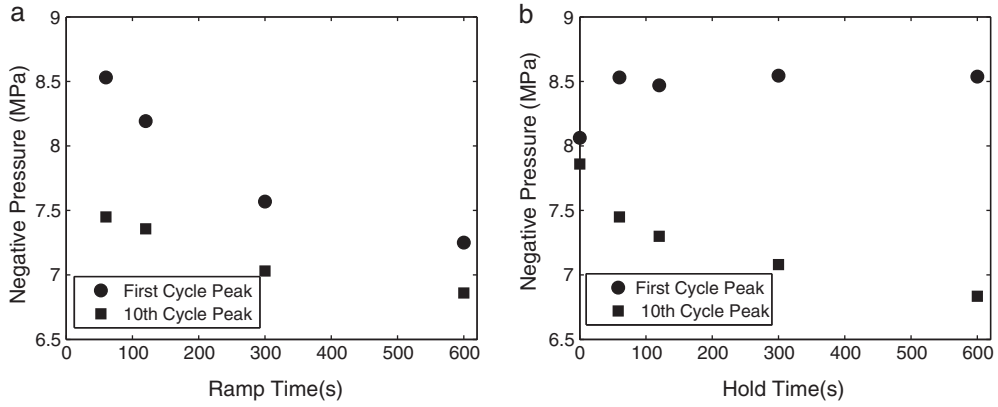

Fig. 16. Peak negative pressure in the membrane during the first and tenth cycle of hygro-thermal cyclic loading (a) as a function of ramp time with 60 s hold time (b) as a function of hold time with 60 s ramp time.

this obviously cannot be matched to that of an actual fuel cell. The most extreme form of loading would be to hold at the hydrated state but not at the dried state; 60 s would probably be a sufficient hold time.

6. Conclusions

The behavior of Nafion was explored via experiments under partially constrained swelling conditions and via simulation under partially constrained swelling and fuel cell constrained conditions. A three-dimensional hygro-thermal elastic–viscoplastic constitutive model developed for Nafion based on uniaxial tensile data and previously shown to be valid for biaxial loading was used for the simulations via a finite element implementation.

Bimaterial strip swelling was used to probe the partially constrained swelling behavior of Nafion. When the strip was hydrated the membrane swelled causing the strip to curl with the membrane on the convex side until the force from the membrane was balanced by a moment in the GDL. A compressive plastic deformation occurs in the membrane which then results in a small tensile stress upon drying which gives a slight curvature of the bilayer with the membrane on the concave side after drying. The ratio between the hydrated radii of the two bilayers with different thicknesses of Nafion were found to agree with those predicted by a simple modification of the Stoney formula which relies on the assumption that the entire membrane has yielded. The hydrated and dried radii were found to agree with the finite element simulation predictions for two thicknesses of Nafion to within experimental error.

The model was then used to simulate a simplified fuel cell cycle. The particular hygro-thermal cycles chosen were not meant to precisely duplicate those of an operating fuel cell, but rather to demonstrate the power of a three dimensional constitutive model and assess potential mechanical damage mechanisms. Simulations of this nature are useful in guiding startup and shutdown procedures for fuel cells, for designing/validating potential procedures for accelerated lifetime testing, and for designing alternative fuel cell geometries. The findings of previous researchers were confirmed that a tensile stress arises in the plane of the membrane upon drying. Further, a negative hydrostatic pressure develops in the channel suggesting a driving force for cavitation or crazing. A study of the effect of ramp rate and hold time revealed a significant time dependence of the pressure, which is not surprising given the significant rate dependence observed for Nafion under uniaxial mechanical loading. The model could be further strengthened with the inclusion of a set of failure criteria. Many researchers have begun to evaluate membrane failure including such methods as strain to break [17], knife slit [18], trouser tear, double edged notched tension [19], creep rupture [20], and pressure-loaded blister test [15,21]. With further advancements information from one or several of these could be incorporated into the constitutive model.

Acknowledgements

Funding for this work was provided by an MIT Presidential Fellowship, an MIT Martin Environmental Fellowship, NSF grant CMMI-0700414, and the Masdar Institute.

References

[1] R. Borup, J. Meyers, B. Pivovar, Y. Kim, R. Mukundan, N. Garland, D. Myers, M. Wilson, F. Garzon, D. Wood, P. Zelenay, K. More, K. Stroh, T. Zawodzinski, J. Boncella, J. McGrath, M. Inaba, K. Miyatake, M. Hori, K. Ota, Z. Ogumi, S. Miyata, A. Nishikata, Z. Siroma, Y. Uchimoto, K. Yasuda, K. Kimijima, N. Iwashita, Chemical Reviews 107 (2007) 3904–3951.
[2] Y. Lai, C. Mittelsteadt, C. Gittleman, D. Dillard, Journal of Fuel Cell Science and Technology 6 (2009) 021002-1–021002-13.
[3] M. Silberstein, M. Boyce, Journal of Power Sources 195 (2010) 5692–5706.
[4] M. Silberstein, P. Pillai, M. Boyce, Polymer, in press, doi:10.1016/j.polymer.2010.11.032.
[5] A. Herrmann, MS thesis, Massachusetts Institute of Technology, Cambridge, MA, 2006, February.
[6] Y. Li, D. Dillard, Y.H. Lai, S. Case, M. Ellis, C. Gittleman, Society for Experimental Mechanics - SEM Annual Conference and Exposition on Experimental and Applied Mechanics 1 (2009) pp. 332-333.
[7] L. Freund, S. Suresh, Thin Film Materials: Stress Defect Formation and Surface Evolution, Cambridge University Press, 2003.
[8] M. Satterfield, J. Benziger, Journal of Physical Chemistry B 112 (2008) 3693–3704.
[9] Y. Tang, M. Santare, A. Karlsson, S. Cleghorn, W. Johnson, Journal of Fuel Cell Science and Technology 3 (2006) 119–124.
[10] A. Kusoglu, A. Karlsson, M. Santare, S. Cleghorn, W. Johnson, Journal of Power Sources 161 (2006) 987–996.
[11] A. Kusoglu, M. Santare, A. Karlsson, S. Cleghorn, W. Johnson, Journal of The Electrochemical Society 157 (2010) B705–B713.
[12] R. Solasi, Y. Zou, X. Huang, K. Reifsnider, D. Condit, Journal of Power Sources 167 (2007) 366–377.
[13] H. Gasteiger, M. Mathias, Proceedings of the Proton Conducting Membrane Fuel Cells III 2002 (2005) 1–24.
[14] Y. Lai, P. Rapaport, C. Ji, V. Kumar, Journal of Power Sources 184 (2008) 120–128.
[15] Y. Li, D. Dillard, S. Case, M. Ellis, Y. Lai, C. Gittleman, D. Miller, Journal of Power Sources 194 (2009) 873–879.
[16] X. Haung, R. Solasi, Y. Zou, M. Feshler, K. Reifsnider, D. Condit, S. Burlatsky, T. Madden, Journal of Polymer Science Part B: Polymer Physics 44 (2006) 2346–2357.
[17] Y. Tang, A. Karlsson, M. Santare, M. Gilbert, S. Cleghorn, W. Johnson, Materials Science and Engineering A 425 (2006) 297–304.
[18] K. Patankar, D. Dillard, S. Case, M. Ellis, Y. Li, Y. Lai, M. Budinski, C. Gittleman, Journal of Polymer Science Part B—Polymer Physics 48 (2010) 333–343.
[19] Y. Li, J. Quincy, S. Case, M. Ellis, D. Dillard, Y. Lai, M. Budinski, C. Gittleman, Journal of Power Sources 185 (2008) 374–380.
[20] R. Solasi, X. Huang, K. Reifsnider, Mechanics of Materials 42 (2010) 678–685.
[21] D. Dillard, Y. Li, J. Grohs, S. Case, M. Ellis, Y. Lai, M. Budinski, C. Gittleman, Journal of Fuel Cell Science and Technology 6 (2009) 031014-1–031014-8.